Study of the metal ion adsorption capacity of palygorskite by computer simulation

CHUAN-WEN LIU[1]*, MIN-HSIEN LIU[2], TO-MAI WANG[3], CHENG-LUNG CHEN[4]
and TZU-HAO TING[1]

[1]*Department of Chemistry, R.O.C Military Academy, Kaohsiung City, Taiwan, ROC,*
[2]*Department of Chemical and Materials Engineering, Chung-Cheng Institute of Technology, National Defense University, Taoyuan 335, Taiwan, ROC,* [3]*Institute of Nuclear Energy Council, ROC and* [4]*Department of Chemistry, National Sun Yat-sen University, Kahsiung 804, Taiwan, ROC*

Abstract: Palygorskite is a magnesium-rich aluminosilicate clay mineral with a unique chain-layered structure. This structure gives palygorskite a large specific surface area and interesting physical properties. Many researchers have investigated the applications of palygorskite in various fields, including heavy metal adsorption, petroleum and chemical industries, building materials, medicine and agriculture. In this study, molecular dynamics simulations were used to explore the heavy metal adsorption ability of palygorskite. The results showed that polyacrylic acid (PAA) had a heavy metal adsorption ability. In terms of the ability of the substrate to adsorb Pb^{2+}, Ni^{2+} and Cr^{3+}, palygorskite (attapulgite, ATP) was more effective than SiO_2 or clay. Based on this study, the same phenomenon reported in the literature was confirmed, and it was demonstrated that molecular dynamics could properly simulate the filtration of heavy metal ions in water using novel materials. Moreover, H^+ was found to play an essential role in assisting PAA/ATP in capturing heavy metal ions. Using this method, we were able to observe the details of heavy-ion adsorption.

Keywords: palygorskite; molecular dynamics; heavy metal adsorption; polyacrylic acid.

INTRODUCTION

Palygorskite or attapulgite (ATP) is a typical clay soil found throughout the world, with the chemical formula $(Mg,Al)_2Si_4O_{10}(OH)\cdot4(H_2O)$. Scientists have noted its unique properties and particular chain-layer structure. Numerous res-

earchers have used ATP in experiments or modified it to improve its properties to expand its application. For example, ATP can be used in heavy metal adsorption, the petroleum and chemical industries, building materials, medicine and agriculture. Rusmin *et al.* developed a simple method for the preparation of a magnetic chitosan-palygorskite nanocomposite that showed excellent effects in terms of removing Pb^{2+} from water; after four adsorption–desorption cycles, it still had an 82% capability.[1] Eleni *et al.* presented a method to remove Ca^{2+} from water using sodium-treated ATP and proposed a kinetic model to explain their experimental results.[2] Wei *et al.* synthesized attapulgite-maintained nanoscale zero-valent iron. Their experimental results confirmed that introducing ATP increased the Cr(VI) removal efficiency.[3] In another study, Ma *et al.* presented a novel method for synthesizing a new material, a polydopamine-modified attapulgite-supported nanosized zero-valent iron composite. The new material reduced the toxicity of Cr (VI) in the solution, and the results showed that ATP played a significant role in this process.[4] Using hydrothermal ATP, Zhang *et al.* demonstrated that benzene, naphthalene and phenanthrene could all be effectively removed after special treatment.[5] Câmara presented the application of ATP in adsorptive desulfurization in petroleum refining, which produced excellent results regarding the adsorption of sulfur compounds in actual diesel fuel.[6] Zhai *et al.* reported that methylene blue-adsorbed palygorskite could effectively degrade bisphenol A over a wide pH range from 3 to 9 through carbonization. Additionally, it can eliminate organic pollutants.[7] Mavrikos *et al.* prepared a novel material with natural ATP and TiO_2, Zn and Cu and demonstrated excellent results for the adsorption of air pollution.[8] Using ATP and wood fiber, Zhou *et al.* prepared an aerogel material with excellent mechanical properties and the ability to self-adjust to humidity.[9] By combining nano clay minerals (ATP) and rigid polyurethane foams, Wang *et al.* created a novel material that enhanced the thermal insulation performance of building materials.[10] Chalvatzi *et al.* found that ATP dietary supplementation could render cecal microbial profiles more homogeneous at the start of lactation and enable more efficient butyrate production.[11] Wang *et al.* presented an embodiment of palygorskite as a medicine carrier and showed that its plasticity and liquidity limits were promising.[12] Yong *et al.* used ATP's ion adsorption properties to capture Cr in alkaline soil with cadmium pollution.[13] Shao *et al.* prepared a new nanoparticle composite in which Pd/Fe was supported on organic ATP to address soil pollution. This composite removed 4,4'-dibrominated diphenyl ether effectively.[14] Zhou *et al.* prepared composite polyacrylic acid (PAA) and ATP (PAA/ATP) to adsorb Pb^{2+}, Ni^{2+} and Cr^{3+}.[15] All these studies showed a different adsorption ability of ATP and its composites. In an earlier simulation in our laboratory, a technical method was used for the liquid chromatographic separation of explosive molecules, and it was a success in that simulation.[16] Prior to this research, we hypothesized that PAA/ATP would adsorb heavy metal ions

but did not know whether PAA or ATP adsorbed more strongly. This was the aim of our study, which we addressed via successful simulation. This study simulated PAA composites of SiO_2 (PAA/Si) and clay (PAA/clay). The adsorption abilities of these composites were compared with those of PAA/ATP described in Zhou's report. Our goal was to demonstrate that simulation, at least qualitatively, predicts complicated composites' adsorption abilities.

THEORY AND METHODS

The Material Studio 6.0 package was used to model these systems in this simulation. In addition, the molecular dynamics (MD) simulation Forcite-calculation module was used to investigate the adsorption of ions by the composites. The adsorption of Pb^{2+}, Ni^{2+} and Cr^{3+} by PAA/ATP was experimentally simulated.[15] A similar simulation method was also used to investigate PAA/SiO_2 and PAA/clay systems.

In this study, molecular dynamics (MD) simulation with the Universal Force Field[17] (UFF) was adopted to carry out the computations.

In UFF, the interaction energy is:

$$E = E_R + E_\theta + E_\varphi + E_w + E_{vdw} + E_{el} \tag{1}$$

where E is the potential energy, E_R is the bond stretching energy, E_θ and E_φ are the angular distortions, E_w is the inversion term, E_{vdw} is the nonbonded interaction energy and E_{el} is the electrostatic term. The interaction force and acceleration of each atom are:

$$\vec{F}_i = m_i \vec{a}_i \tag{2}$$

$$\vec{a}_i = -\nabla_i E \tag{3}$$

The atomic position and velocity were obtained by numerically solving the Newtonian equation by the Verlet method:

$$\vec{v}\left(t + \frac{1}{2}\delta t\right) = \vec{v}\left(t - \frac{1}{2}\delta t\right) + \vec{a}(t)\delta t \tag{4}$$

$$\vec{r}_i(t + \delta t) = \vec{r}_i(t) + \vec{v}\left(t + \frac{1}{2}\delta t\right)\delta t \tag{5}$$

In our simulation, the conventional MD method was adopted, and the system was simulated to reach thermal equilibrium:

$$K.E \sim \frac{3}{2} NkT \tag{6}$$

After the system was well equilibrated, further simulations were carried out to collect trajectories for subsequent analysis.

Different radial distribution functions (RDFs) can be calculated using Eq. (7) to analyze the simulation results:

$$g(r) = \frac{dn_r}{\rho 4\pi r^2 dr} \tag{7}$$

where dn_r is the number of atoms distributed in $r \rightarrow r + dr$, and ρ is the bulk density. RDF, $g(r)$, is the probability of an atom being at a distance r from another tagged atom. It shows a

significant probability of probable distance ranges. RDF analyzes atom distributions in the solid, liquid and gas phases.

This research examined four different systems: PAA/ATPno, with the ATP surface treated with the PAA functional group in a neutral solution; PAA/ATPH, with the ATP surface treated with the PAA functional group in an acidic solution; PAA/Sino, with the SiO_2 surface treated with the PAA functional group in neutral solution; and PAA/Clayno, with the clay surface treated with the PAA functional group in neutral solution. All four systems contained the same ratios of heavy metal ions Pb^{2+}, Ni^{2+} and Cr^{3+}. Table I displays the components for each of the four systems.

TABLE I. Composition of modeled systems

Property	PAA/ATPno	PAA/ATPH	PAA/Sino	PAA/Clayno
Pb^{2+}	30	50	30	30
Ni^{2+}	30	50	30	30
Cr^{3+}	30	50	30	30
Cl^-	90	150	90	90
NO_3^-	120	200	120	120
H_2O	3300	3300	3300	3300
H^+	–	300	–	–
Substrate	ATP (palygorskite, attapulgite)		SiO_2 (quartz)	Clay (kaolinite)
Density of solution, g/cm³	1.0	1.0	1.0	1.0
Box size, Å³	52×51×90	52×51×100	50×51×87	51×45×90

In this simulation, SiO_2 and clay were also selected as substrates through the same Si atom in their structures. The three-dimensional structure of ATP was adopted from the Inorganic Crystal Structure Database (ICSD) No. 185485[18] and the literature.[19] The 3D structures of SiO_2 and clay were also obtained from the ICSD. The structures are shown in Fig. 1 (a, b and c).

The surfaces of the substrates were covered with polyacrylic acid $((C_3H_4O_2)_n$, $n = 5)$. In this simulation, PAA was synthesized from polyacrylic acid and modified ATP. In the first step, modified ATP was formed by putting ATP into 3-mercapto-1-propane sulfonic acid sodium $(C_3H_7O_3S_2Na$, MPS). In the second step, polyacrylic acid was added to the modified ATP, and the polymerization process was conducted. PAA was therefore obtained via two steps in this experiment; the final 3D structure of PAA is shown in Fig. 1d.[15]

To build the PAA/ATP, PAA/SiO₂, and PAA/Clay systems, 10 PAA molecules were evenly distributed on the surface of the clay, ATP and SiO_2. Solutions of PAA/ATPno, PAA/ATPH, PAA/SiO₂ and PAA/clay were mixed in the amorphous cell module at a density of 0.3 g/cm³. Next, the systems were simulated to their thermal equilibrium states, after which they were compressed slightly (3 %), and an MD simulation was carried out until a new thermal equilibrium was reached. The above steps were repeated until the system density was 1.0 g/cm³. After this stage, an MD simulation of 10,000 fs was performed to ensure that the solutions were well mixed. Then, these solutions were placed on top of the substrates, and an MD simulation of 1,000,000 fs in each system was performed to stabilize the systems. Snapshots of the system are shown in Fig. 2.
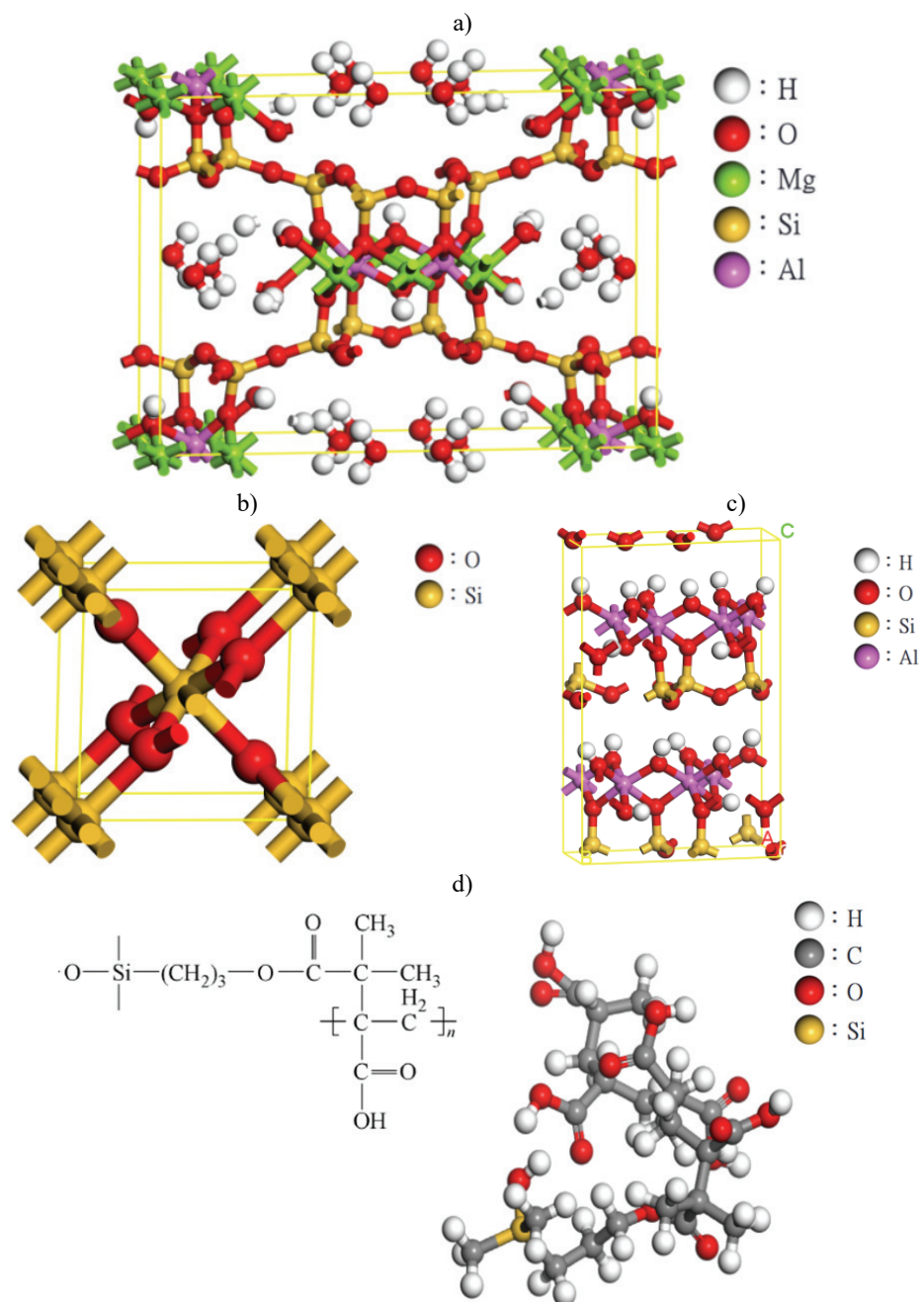
Fig. 1. 3D structure of: a) ATP, b) SiO$_2$, c) clay and d) PAA.
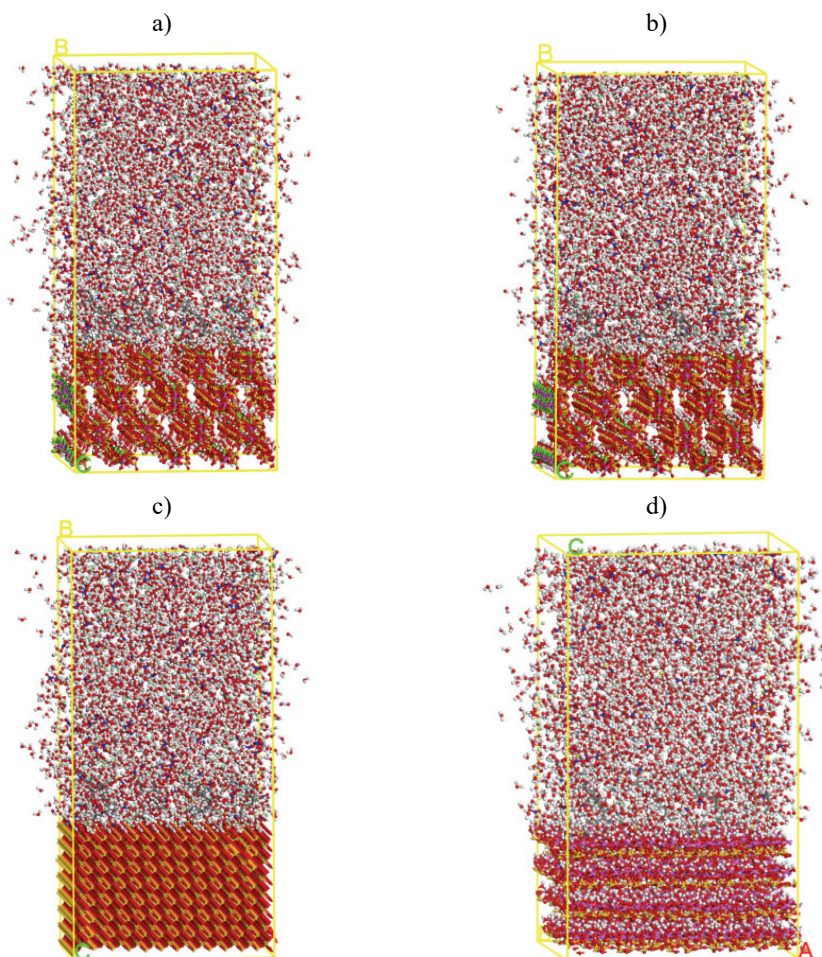
a)

b)

c)

d)

Fig. 2. Simulation model of the: a) PAA/ATPno, b) PAA/ATPH, c) PAA/Sino and
d) PAA/Clayno systems.

RESULTS AND DISCUSSION

The results from the literature showed the adsorption ability of the PAA/ /ATP substrate in an acidic solution to be Pb^{2+} (35 mg g^{-1}) > Cr^{3+} (16 mg g^{-1}) > Ni^{2+} (2 mg g^{-1}).[15] Fig. 3 shows the calculated RDFs of O in the PAA molecule to ions in the PAA/ATPH system. Fig. 3 shows that the corresponding peak intensities were 7.2 for Pb^{2+} at 2.7 Å, 5.8 for Cr^{3+} at 2.3 Å and 4.4 for Ni^{2+} at 2.3 Å. These peaks indicate that the simulated amounts of adsorption ions were in the same order as reported in the literature. Therefore, the correct results obtained using our simulation showed that the modeling method is appropriate for these composite systems.
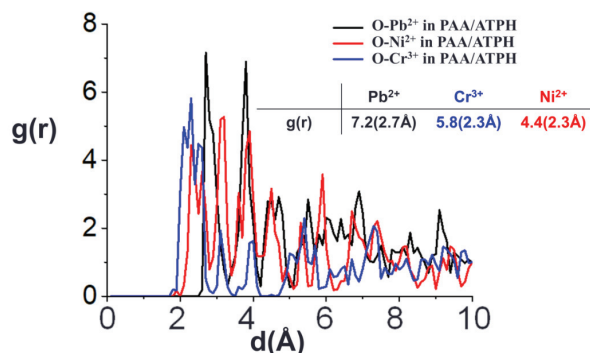
Fig. 3. RDF of O(PAA)–M$^+$ in the PAA/ATPH system.

Similar analyses were carried out for the other composite systems. The simulated RDFs are shown in Table II. The adsorption abilities were Ni^{2+} (10.1) > Pb^{2+} (6.2) > Cr^{3+} (4.6) for the PAA/ATPno system, Cr^{3+} (15.3) > Pb^{2+} (11.9) > Ni^{2+} (2.5) for the PAA/Sino system, and Cr^{3+} (52.3) > Pb^{2+} (5.5) > Ni^{2+} (5.1) for the PAA/Clayno system. In the PAA/Sino system, the adsorption capacities for Cr^{3+} (15.3) and Pb^{2+} (11.9) were more significant than those for Ni^{2+} (2.5). In the PAA/Clayno system, the adsorption capacity for Cr^{3+} (52.5) was more significant than that for Pb^{2+} (5.1) and Ni^{2+} (5.5).

TABLE II. RDF analyses of O (PAA) to M$^+$ and O (water) to M$^+$ in the four systems

System	O(PAA)···M$^+$			O(water)···M$^+$		
	Pb^{2+}	Cr^{3+}	Ni^{2+}	Pb^{2+}	Cr^{3+}	Ni^{2+}
PAA/ATPH	7.2 (2.7Å)	5.8 (2.3Å)	4.4 (2.2Å)	1.8 (3.0Å)	2.9 (2.2Å)	2.4 (1.9Å)
PAA/ATPno	6.2 (2.7Å)	4.6 (2.0Å)	10.1 (2.0Å)	2.3 (2.9Å)	4.7 (2.0Å)	2.3 (2.9Å)
PAA/Sino	11.9 (2.9Å)	15.3 (1.8Å)	2.5 (1.8Å)	1.9 (3.0Å)	4.0 (2.0Å)	3.1 (2.0Å)
PAA/Clayno	5.1 (2.7Å)	52.3 (1.8Å)	5.5 (2.0Å)	2.1 (3.1Å)	3.1 (2.2Å)	4.6 (2.0Å)

As presented in Table II, the RDF of the M$^+$ to O (water) in the liquid system shows that the order of adsorption capacity was the same for all four systems: Cr^{3+} > Ni^{2+} > Pb^{2+}. As Cr^{3+} is the most significant positively charged ion, it attracts more O (water) than the other two ions. According to the literature, the hydrated radius of Ni^{2+} is 0.69 Å[20] and that of Pb^{2+} is 1.19 Å.[21] Therefore, O (water) is closer to Ni^{2+} than Pb^{2+}, and the number of neighboring water molecules around Ni^{2+} was more significant than that around Pb^{2+}.

In Table II, the RDF of O(PAA)–M$^+$ in the PAA/ATPno, PAA/ATPH, PAA//Sino and PAA/Clayno systems showed that the adsorption capacity for the Pb^{2+} by the PAA polymer was of the order: PAA/Sino > PAA/ATPH > PAA/ATPno > PAA/Clayno. The order for Ni^{2+} was: PAA/ATPno > PAA/Clayno > PAA//ATPH > PAA/Sino. The order for Cr^{3+} was: PAA/Clayno > PAA/Sino > PAA/

/ATPH > PAA/ATPno. These results showed that the most significant adsorption number of O(PAA)–Pb^{2+} was observed in the PAA/Sino system, the most significant adsorption number of O(PAA)–Ni $^{2+}$ was in PAA/ATPno, and the most significant adsorption number of O(PAA)–Cr^{3+} was in PAA/Clayno.

Fig. 4 shows the RDF of O (PAA) in the four systems. In the dynamic snapshot, the peak at 0.61–0.69 Å represented =O and –O in the COOH functional group. It has been shown that the distance between the O atoms in the –COOH group decreased in the PAA/ATPH, PAA/Sino and PAA/Clayno systems. It was also observed that M$^+$ had a greater possibility of moving close to the –COOH group, causing the phenomenon that =O and –O became closer to each other in the RDF analysis. In addition, the M$^+$ in the PAA/ATP system did not show this phenomenon. The peak at 2.27–2.29 Å was the normal RDF of O atoms in the –COOH functional group in the four systems. However, the PAA/ATPH system had two peaks of low intensity of 2.81 and 4.65 Å, which showed that the PAA molecules in the PAA/ATPH system had the possibility of getting closer to each other. This phenomenon was most evident in the PAA/ATPH system of the four systems.
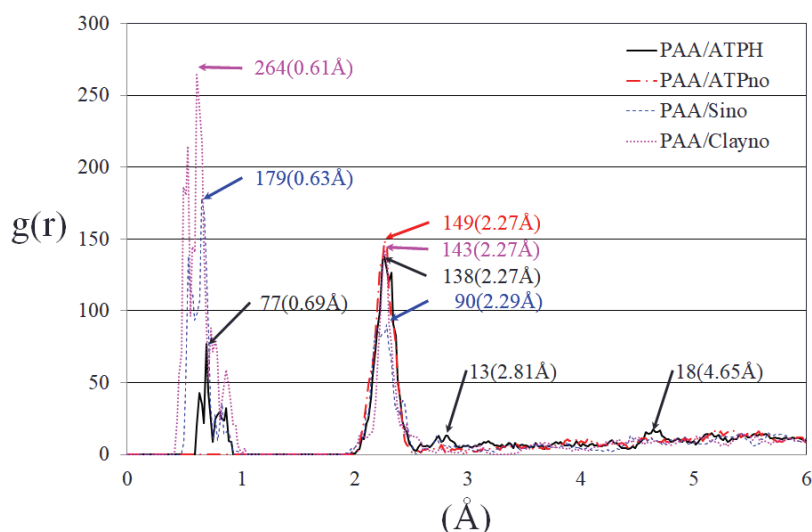

Fig. 4. RDF analysis of O (PAA) in the four systems.

The above analysis showed the adsorption of metal ions by PAA. In addition, we were also interested in the adsorption site of the polymer. By analyzing 101 frames of trajectories in 10 ps, Pb^{2+}, Ni^{2+} and Cr^{3+} near the surface of the substrates within 10 Å were counted, as shown in Fig. 5. This shows the number of heavy metal ions trapped by PAA/substrate. The count of heavy metal ions

inside the PAA molecule differed from the results of the RDF analysis of heavy metal ions and the O atom of the PAA molecule.

On the other hand, the PAA/ATPH system had the most of Pb^{2+} inside the PAA molecule. The PAA/ATPno system was the best for Cr^{3+}, and the PAA//ATPH system still proved the most effective in terms of capturing Ni^{2+} in comparison with the other systems. The PAA/Clayno system could have shown better results regarding the numbers inside the PAA molecule for heavy metal ions. However, the RDF results showed that the PAA/Clayno system had excellent adsorption of Cr^{3+}. One possible reason for this result was that the heavy metal ions were adsorbed by the –COOH group on the PAA molecule, showing that this –COOH group played an essential role in the adsorption of heavy metal ions. The clay substrate had little effect on the adsorption of heavy metal ions.
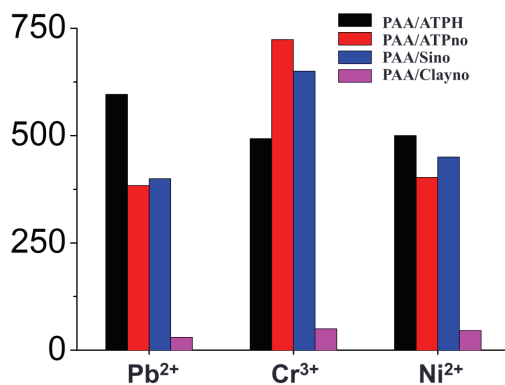

Fig. 5. Analysis of ions inside the PAA molecular chain in the PAA/ATPH, PAA/ATPno, PAA/Sino and PAA//Clayno systems.

According to the PAA/Clayno system data in Fig. 5, the trajectory of the Cr^{3+} near the clay was analyzed, as shown in Fig. 6. The resulting analysis showed that the PAA/Clayno dynamic simulation trajectory in 5 ps included 5000 steps and 51 frames. In the Cr^{3+} trajectory, it was almost wandering in a cube with a side length of 0.6 Å. Therefore, Fig. 6 might provide strong evidence to support the conclusion, shown in Fig. 5, that Cr^{3+} near the surface of the clay substrate within 10 Å were almost captured by the –COOH group and occupied the site of the –COOH group's activity. As a result, the low number of ions present in the PAA molecular chain of the PAA/Clayno system, depicted in Fig. 5, caused a significant difference in the RDF of O (PAA)–Cr^{3+}, as shown in Table II. This may be a type of fouling of the PAA molecules in the PAA/Clayno system.

CONCLUSION

ATP is a clay mineral with expanding applications owing to the development of technology. In this research, a 3D model of ATP was built to simulate its beh-
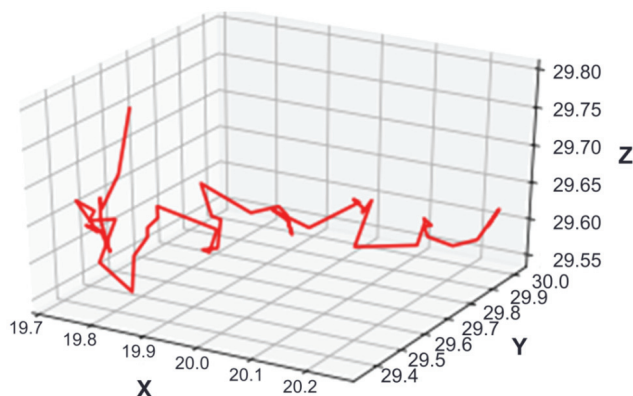
Fig. 6. Trajectory of Cr^{3+} near the surface of the clay substrate within 10 Å.

avior. Modeling research would assist in follow-up ATP research. According to the results, PAA molecules have excellent adsorption ability. The ability of the systems with PAA added to the substrate to adsorb Pb^{2+}, Ni^{2+} and Cr^{3+} was in the order ATP > SiO_2 > clay. In comparing the four systems, PAA/ATPno proved the most effective in adsorbing the Ni^{2+}, while for adsorbing Pb^{2+}, PAA/Sino was the best among the four systems. On the other hand, PAA/Clayno was the most effective at adsorbing the Cr^{3+}. For both Pb^{2+} and Cr^{3+}, the PAA/Sino system is the most efficient of the four systems. Furthermore, the H^+ evenly disperses the PAA molecules to improve the ability of the PAA/ATP system to adsorb heavy metal ions such as Pb^{2+}, Ni^{2+} and Cr^{3+}. According to the results of this simulation, the PAA/ATPH system has an excellent ability to adsorb heavy metal ions. This simulation could help advance research in nanotechnology and its application in ATP.

И З В О Д

ПРОУЧАВАЊЕ АДСОРПЦИОНОГ КАПАЦИТЕТА ПАЛИГОРСКИТА ПРЕМА МЕТАЛНИМ ЈОНИМА РАЧУНАРСКОМ СИМУЛАЦИЈОМ

CHUAN-WEN LIU[1], MIN-HSIEN LIU[2], TO-MAI WANG[3], CHENG-LUNG CHEN[4] и TZU-HAO TING[1]

[1]Department of Chemistry, R.O.C Military Academy, Kaohsiung City, Taiwan, ROC, [2]Department of Chemical and Materials Engineering, Chung-Cheng Institute of Technology, National Defense University, Taoyuan 335, Taiwan, ROC, [3]Institute of Nuclear Energy Council, ROC и [4]Department of Chemistry, National Sun Yat-sen University, Kahsiung 804, Taiwan, ROC

Палигорскит је минерал алуминосиликатне глине богат магнезијумом са јединственом ланчаном слојевитом структуром. Ова структура даје палигорскиту велику специфичну површину и занимљива физичка својства. Многи истраживачи су истраживали примену палигорскита у различитим областима, укључујући адсорпцију тешких метала, индустрију нафте, хемијску индустрију, грађевинске материјале, медицину и пољоприв-

реду. У овој студији, коришћене су симулације молекулске динамике за истраживање способности палигорскита за адсорпцију тешких метала. Резултати су показали да поли-акрилна киселина (PAA) има способност адсорпције тешких метала. Као супстрат за адсорбовање Pb^{2+}, Ni^{2+} и Cr^{3+}, палигорскит (атапулгит, ATP) је био ефикаснији од SiO_2 или глине. На основу ове студије потврђен је исти феномен описан у литератури и показано је да молекулска динамика може правилно симулирати филтрацију јона тешких метала у води користећи нове материјале. Штавише, откривено је да H^+ игра кључну улогу у помагању PAA/ATP у хватању јона тешких метала. Користећи ову методу, могли смо да посматрамо детаље адсорпције тешких јона.

REFERENCES

1. R. Rusmin, B. Sarkar, R. Mukhopadhyay, T. Tsuzuki, Y. Liu, R. Naidu, *J. Colloid Interface Sci.* **608** (2022) 575 (https://doi.org/10.1016/j.jcis.2021.09.109)
2. G. Eleni, P. Georgios, K. Konstantina, B. Alexandros, *Water Supply* **22** (2022) 156 (https://doi.org/10.2166/ws.2021.283)
3. Y. Wei, M. Usman, M. Faroop, M. Adeel, F. U. Haider, Z. Pan, W. Chen, H. Liu, L. Cai, *Water, Air, Soil Poll.* 233 (2022) 48 (https://doi.org/10.1007/s11270-022-05513-z)
4. B. Ma, J. Yao, Z. Chen, B. Liu, J. Kim, C. Zhao, X. Zhu, V. G. Mihucz, T. Minkina, T. S. Knudsen, *Chemosphere* **287** (2022) 131970 (https://doi.org/10.1016/j.chemosphere.2021.131970)
5. S. Y. Zhang, Y. L. Zhang, X. S. Su, Y. Zhang, *Chem. Res. Chin. Univ.* **29** (2013) 37 (https://doi.org/10.1007/s40242-013- 2303-8)
6. A. B. F. Câmara, R. V. Sales, L. C. Bertolino, R. P. P. Furlanetto, E. Rodriguez-Castellón, L. S. de Carvalho, *Adsorption* **26** (2020) 267 (https://doi.org/10.1007/s10450-019-00144-z)
7. P. Zhai, H. Liu, F. Sun, T. Chen, X. Zou, H. Wang, Z. Chu, C. Wang, M. Liu, D. Chen, *Appl. Clay Sci.* **216** (2022) 106327 (https://doi.org/10.1016/j.clay.2021.106327)
8. A. Mavrikos, D. Papoulis, N. Todorova, I. Papailias, C. Trapalis, D. Panagiotaras, D. A. Chalkias, E. Stathatos, E. Gianni, K. Somalakidi, D. Sygkridou, S. Komarneni, *J. Photochem. Photobiol., A* **423** (2022) 113568 (https://doi.org/10.1016/j.jphotochem.2021.113568)
9. X. Zhou, H. Jin, A. Gu, X. Li, L. Sun, P. Mao, Y. Yang, S. Ding, J. Chen, S. Yun, *J. Clean. Prod.* **335** (2022) 130367 (https://doi.org/10.1016/j.jclepro.2022.130367)
10. Y. Wang, K. Cui, B. Fang, F. Wang, *Nanomaterials* **12** (2022) 609 (https://doi.org/10.3390/nano12040609)
11. S. Chalvatzi, M. S. Kalamaki, K. Arsenos, P. Fortomaris, *J. Appl. Microbiol.* **120** (2022) 1033 (https://doi.org/10.1111/jam.13041)
12. J. Wu, S. Ding, J. Chen, S. Zhou, H. Ding, *Int. J. Biol. Macromol.* **68** (2014) 107 (https://doi.org/10.1016/j.ijbiomac.2014.04.030)
13. Y. Yong, Y. Xu, Q. Huang, Y. Sun, L. Wang, X. Liang, X. Qin, L. Zhao, *Sci. Total Environ.* **813** (2022) 152636 (https://doi.org/10.1016/j.scitotenv.2021.152636)
14. J. Shao, Y. Zhang, Z. Liu, Z. Fei, Y. Sun, Z. Chen, X. Wen, W. Shi, D. Wang, C. Gu, *Environ. Sci. Pollut. Res.* **29** (2 022) 4461 (https://doi.org/10.1007/s11356-021-15997-7)
15. S. Zhou, A. Xue, Y. Zhang, Q. Wang, M. Li, X. Chu, Y. Zhao, W. Xing, *J. Ind. Eng. Chem. (China)* **66** (2015) 618 (https://doi.org/10.11949/j.issn.0438-1157.20141244)

16. C. W. Liu, B. C. Kuo, M. H. Liu,Y. R. Huang, C. C. Chen, *J. Mol. Graph. Model.* **85** (2018) 331 (https://doi.org/10.1016/j.jmgm.2018.09.009)

17. A. K. Rappe, C. J. Casewit, K. S. Colwell, W. A. Goddard III, W. M. Skiff., *J. Am. Chem. Soc.* **114** (1992) 10024 (https://doi.org/10.1021/ja00051a040)

18. R. Giustetto, R. Compagnoni, *Clay Miner.* **46** (2011) 371 (https://doi.org/10.1180/claymin.2011.046.3.371)

19. L. Boudriche, R. Calvet, B. Hamdi, H. Balard, *Colloids Surfaces, A* **392** (2011) 45 (https://doi.org/10.1016/j.colsurfa.2011. 09.031)

20. I. Mobasherpour, E. Salahi, M. Pazouki, *Arabian J. Chem.* **5** (2012) 439 (https://doi.org/10.1016/j.arabjc.2010.12.022)

21. I. Persson, *Pure Appl. Chem.* **82** (2010) 901 (https://doi.org/10.1351/PAC-CON- 09-10-22).